A hybrid CoOOH-rGO/Fe2O3 photoanode with spatial charge separation and charge transfer for efficient photoelectrochemical water oxidation

Ruifeng Chong[a*], Zhenzhen Wang[a], Jiaqi Lv[a], Jiayue Rong[a], Ling Zhang[a], Li Wang[a], Zhixian Chang[a*], Xiang Wang[b*]

[a] Henan Joint International Research Laboratory of Environmental Pollution Control Materials, Henan Provincial Engineering Research Center of Green Anticorrosion Technology for Magnesium Alloys, College of Chemistry and Chemical Engineering, Henan University, Kaifeng 475004, Henan, China

[b] Chemical Sciences Division and Center for Nanophase Materials Sciences, Oak Ridge National Laboratory, Oak Ridge, TN 37831, United States

* Corresponding authors. E-mail: rfchong@henu.edu.cn (R. Chong), chzx19@henu.edu.cn (Z. Chang), wangxiang@ornl.gov (X. Wang).

Abstract

As a promising photoanode for photoelectrochemical (PEC) water oxidation, hematite (Fe2O3) still suffers from poor charge mobility and serious charges recombination and sluggish surface oxygen evolution kinetics. Herein, a hybrid photoanode of cobalt (oxy)hydroxide coupled with reduced graphene oxide modified Fe2O3(CoOOHrGO/Fe2O3) is well crafted by a facile hydrothermal synthesis with a chelationmediated in-situ growth method. Morphology characterizations indicate rGO forms the internal network among isolated Fe2O3 and CoOOH nanosheets distribute on the

terminal of Fe2O 3, forming a spatial separated nanostructure. The resultant CoOOHrGO/Fe2O3 exhibits an obviously reduced onset potential of ca. 150 mV and a significantly enhanced photocurrent density of 2.56 mA cm -2 at 1.23 V, which is ca. 3.3 times higher than that of bare Fe2O3. Especially, the functions of rGO and CoOOH are studied by using electrochemical impedance spectroscopy, open circuit potentials and intensity modulated photocurrent spectroscopy. It is found rGO act as conductive network which facilitates the electron transfer from Fe2O3 to the substrate, while CoOOH evidently passivate the surface states of Fe2O3, improve charge separation and provide catalytic active sites for water oxidation. The spatial charge separation and charge transfer caused by CoOOH and rGO are responsible for the enhanced PEC performance of water oxidation. The rational design and the facile fabrication strategy exhibit great potential to be used for other PEC system with great efficiency.

Keywords hematite; CoOOH; rGO; photoelectrochemical water oxidation; charge separation

1. Introduction

Since Fujishima and Honda firstly reported the concept of photoelectrolysis of water over rutile TiO_2 electrode[1], photoelectrocatalytic (PEC) water splitting into hydrogen and oxygen has gained substantial interests due to it can not only produce renewable energy by harvesting energy directly from sunlight but also reduce the utilize of fossil fuels. So far, several photoanode materials, such as WO_3, $BiVO_4$ and Fe_2O_3, have been extensively developed.[2-4] Among them, Fe_2O_3 is considered as the most promising photoanode material owing to its suitable band gap (~2.1 eV), elemental abundance, non-toxicity and high stability in alkaline solution. However, Fe_2O_3 is still suffers from the poor conductivity, the short hole-diffusion length, short minority carrier lifetime, serious surface recombination and sluggish oxygen evolution reaction (OER) kinetics.[5]

To alleviate the abovementioned challenges, extensive efforts have been devoted to promoting the charge separation and the charge transfer of Fe_2O_3, including morphology control, foreign element doping, heterojunction constructing or oxygen evolution catalyst (OEC) loading. [5] Among these well-designed strategies, OEC loading has been generally demonstrated as an efficient strategy.[7] Many low-cost 3*d* transition metal oxides (NiO, Co_3O_4, $NiFeO_x$ and $CoFeO_x$),[8-12] hydroxides ($Co(OH)_X$, $Ni(OH)_2$ and $NiFe(OH)_x$),[8-12] (oxy)hydroxides (NiOOH, CoOOH and

NiFeOOH),[17-21] phosphates (CoPi, NiPi and NiFePi),[22-24] phosphides (FeP and Ni_2P)[25-27] and layered double hydroxides (CoAl-, CoMn-, NiFe-, ZnCo- and NiCoAl- LDHs)[25-27] *etc.*, have been developed as cocatalysts to improve the PEC performance of Fe_2O_3. Previous reports indicate the mechanism for such OECs promoting PEC water splitting on Fe_2O_3 is mainly attributed to the enhanced holes transfer. Nevertheless, as the counter of holes transfer, the electrons flow from bulk Fe_2O_3 to the substrate have attracted little attention. Several efforts have been carried out to mediate the electron transport. For example, Au and Pt have been reported as electron-transfer benign underlayer to improve PEC water oxidation over Fe_2O_3.[36,37] Reduced graphene oxide (rGO), possessing excellent electrical conductivity (>15000 $cm^2\ V^{-1}\ s^{-1}$), could act as electron shuttle, thus has great potential to facilitate the electron transport in composite photoelectrodes.[38] For instance, Ning et al. verified rGO could accept photogenerated electrons from TiO_2 and enable fast electron transfer in NiFe-LDH/rGO/TiO_2 photoanode theoretically and experimentally.[39] Sun et al. also concluded rGO played an important role that accelerated the transfer rate of electrons in $BiVO_4$/rGO/NiFe-LDHs.[40] Meng et al. demonstrated the direct evidence that the photogenerated electrons transferred as the mobile carriers from Fe_2O_3 to rGO in the composite of Fe_2O_3 nanoparticles/rGO nanosheet.[38] Whereas, few reports have been conducted with rGO incorporated OECs/Fe_2O_3 photoanode, and the charge transfer mechanism in an rGO and OECs co-incorporated Fe_2O_3 still required an in-depth understanding.

Cobalt (oxy)hydroxide (CoOOH) has recently been identified as a realistic active

species for electrocatalytic oxygen evolution reaction (OER).[41-43] Moreover, trivalent cobalt species have been proved to possess an optimal electronic configuration for the adsorption of reactants.[44,45] Recent studies also indicate CoOOH is also a highly efficient OER cocatalyst for promoting photoelectrochemical (PEC) water oxidation. The approaches for decorating CoOOH could be Ar plasma-exfoliation, photo-assisted electrodeposition and spin-coating. [20,46,47] Recently, we developed a facile chelation-mediated in situ growth method to fabricate ultrathin CoOOH onto Fe_2O_3 photoanode.[48] The resulting CoOOH/Fe_2O_3 exhibited remarkably improved photocurrent density of 2.10 mA cm^{-2} at 1.23 V *vs.* RHE, which is *ca.* 2.8 times that of bare Fe_2O_3, and CoOOH was verified to promote charge separation and holes transfer via passivating surface states and suppressing charge recombination. However, owing to the instinct poor conductivity of Fe_2O_3, the electrons transfer would also be an obstacle that hinder the PEC performance of CoOOH/Fe_2O_3. Herein, aiming to further enhance PEC performance of Fe_2O_3, rGO was applied to modulate the electrons transfer of CoOOH/Fe_2O_3. As expected, the resulting CoOOH-rGO/Fe_2O_3 showed a further enhanced photocurrent density of *ca.* 2.56 mA cm^{-2} (at 1.23 V *vs.* RHE), which is 3.3 and 1.2 times larger than that of bare Fe_2O_3 and CoOOH/Fe_2O_3 respectively. A systematic characterization demonstrates that rGO as a conductive network improve electron transfer and CoOOH suppresses surface charge recombination, promotes holes transfer and provides catalytic active sites for water oxidation. The synergistic effect resulted in a high charge separation efficiency and excellent OER catalytic activity

2. Results and discussion

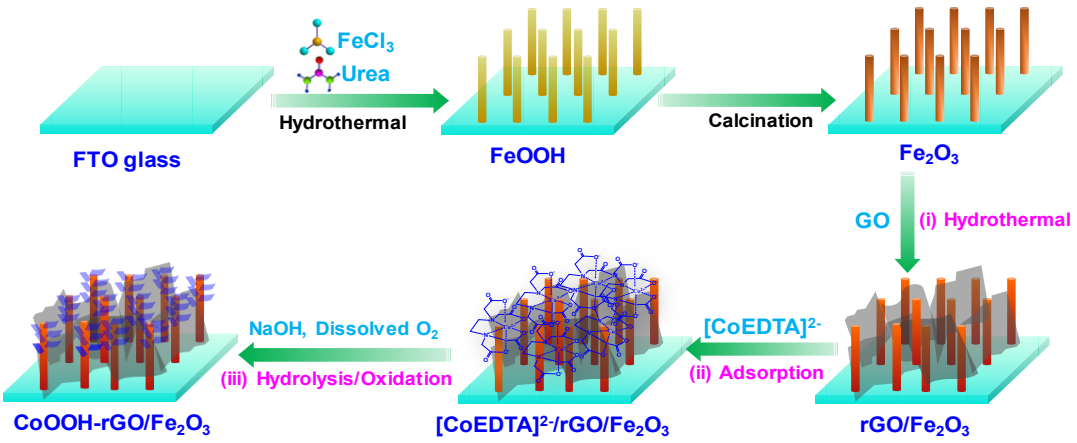

Scheme 1. The fabrication process of CoOOH-rGO/Fe_2O_3 photoanode.

The fabrication process of CoOOH-rGO/Fe_2O_3 is depicted in Scheme 1. Firstly, Fe_2O_3 was fabricated by using a hydrothermal method with $FeCl_3$ and urea as precursor followed by a two-step calcination. Subsequently, rGO and CoOOH were decorated in order with the designed steps, that is, (i) the hydrothermal reaction between GO and Fe_2O_3; (ii) the assembling of Co-EDTA complex on rGO/Fe_2O_3; and, (iii) the hydrolysis of Co-EDTA-rGO/Fe_2O_3 in NaOH solution. In step (i), GO nanosheets were anchored on Fe_2O_3 via the electrostatic interaction between the oxygen functional groups on GO and Fe_2O_3, meanwhile GO were reduced to rGO.[49] The use of EDTA chelates in step (ii) is to enable enough Co species to interact and be loaded on Fe_2O_3. And, at step (iii), Co-EDTA species on rGO/Fe_2O_3 slowly were hydrolyzed and reacted with dissolved oxygen to form CoOOH.[50] Figure 1 shows SEM and/or TEM images for bare Fe_2O_3, rGO/Fe_2O_3, CoOOH/Fe_2O_3 and CoOOH/rGO/Fe_2O_3. The Fe_2O_3 sample appears as nanorods with a diameter of 20-50 nm and a length of *ca*. 200 nm, which vertically stand on FTO substrate (Figure 1a and Figure S1). The GO prepared by a modified Hummers method shows a flake-like structure with wrinkles (~1.0 nm in thickness,

Figure S2). After being decorated on Fe_2O_3, rGO is clearly interwoven among Fe_2O_3 nanorods. As a result, a 3D rGO/Fe_2O_3 network is formed (Figures 1b and 1c; Figure S3). The further deposition of CoOOH on rGO/Fe_2O_3 demonstrates that CoOOH nanosheets with an average lateral size of ~30 nm are vertically deposited on the top of Fe_2O_3 (Figures 1d and 1e). Note, due to the electrostatic repulsion between the oxygen-containing functional groups of rGO with $[Co\text{-}EDTA]^{2-}$, CoOOH prefers to grow on the surface of Fe_2O_3 rather than rGO surface. For comparison, CoOOH/Fe_2O_3 without rGO was synthesized via the chelation-mediated hydrolysis-oxidation method and its morphology feature was shown in Figure 1f. Interestingly, CoOOH on CoOOH/Fe_2O_3 seems much more condensed with larger lateral size compared with those on CoOOH-rGO/Fe_2O_3, which might be attributed to the adjacent rGO limits the continued growth of CoOOH nanosheets. Moreover, the SEM image for the cross-sectional CoOOH-rGO/Fe_2O_3 indicates that CoOOH nanosheets dominate on the top of Fe_2O_3 nanorods to form a tree-like structure (Figure S4). To get more detailed information of the crystalline structure of CoOOH-rGO/Fe_2O_3 composite, the transmission electron microscopy (TEM) was carried out. As seen from TEM images of rGO/Fe_2O_3 and CoOOH-rGO/Fe_2O_3, the isolated Fe_2O_3 is coated by wrinkled and tortuous rGO nanosheets, forming an excellent interfacial contact (Figures 1g and 1h). The length and the width of CoOOH nanosheets are estimated to be 10-30 nm and 6-10 nm respectively, with an average thickness of ~2.6 nm (Figures 1h and 1i). The formed heterojunction between CoOOH and Fe_2O_3 confirms CoOOH directly grew up on Fe_2O_3 surface from high resolution TEM image of CoOOH-rGO/Fe_2O_3 (Figure 1i). The

corresponding lattice fringes of 0.243 nm and 0.220 nm are indexed to (101) and (006) planes of β-CoOOH. TEM results are in line with that of SEM, revealing rGO network plays a crucial role on the morphology of CoOOH nanosheets.

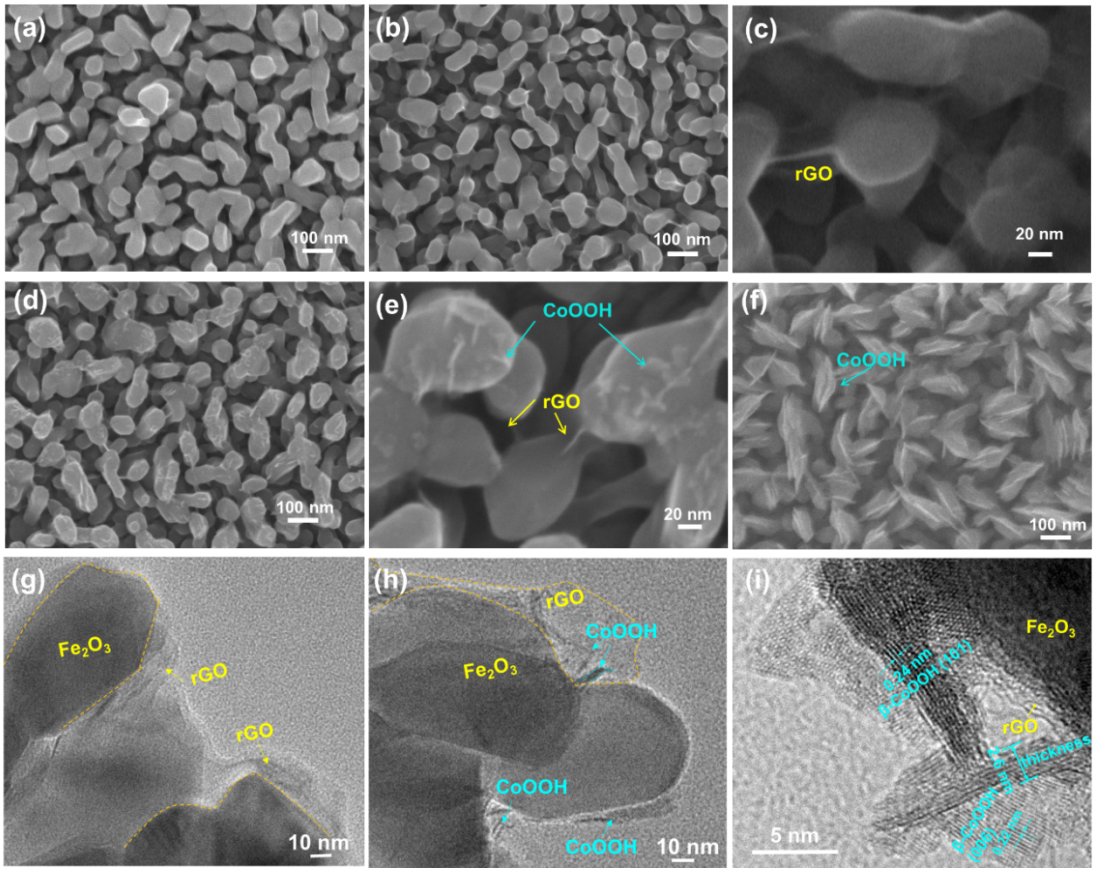

Figure 1 SEM images of (a) Fe_2O_3, (b, c) rGO/Fe_2O_3, (d) CoOOH/Fe_2O_3 and (e, f) CoOOH-rGO/Fe_2O_3; TEM of (h) rGO/Fe_2O_3 and (i) CoOOH-rGO/Fe_2O_3; (j) High resolution TEM image of CoOOH-rGO/Fe_2O_3.

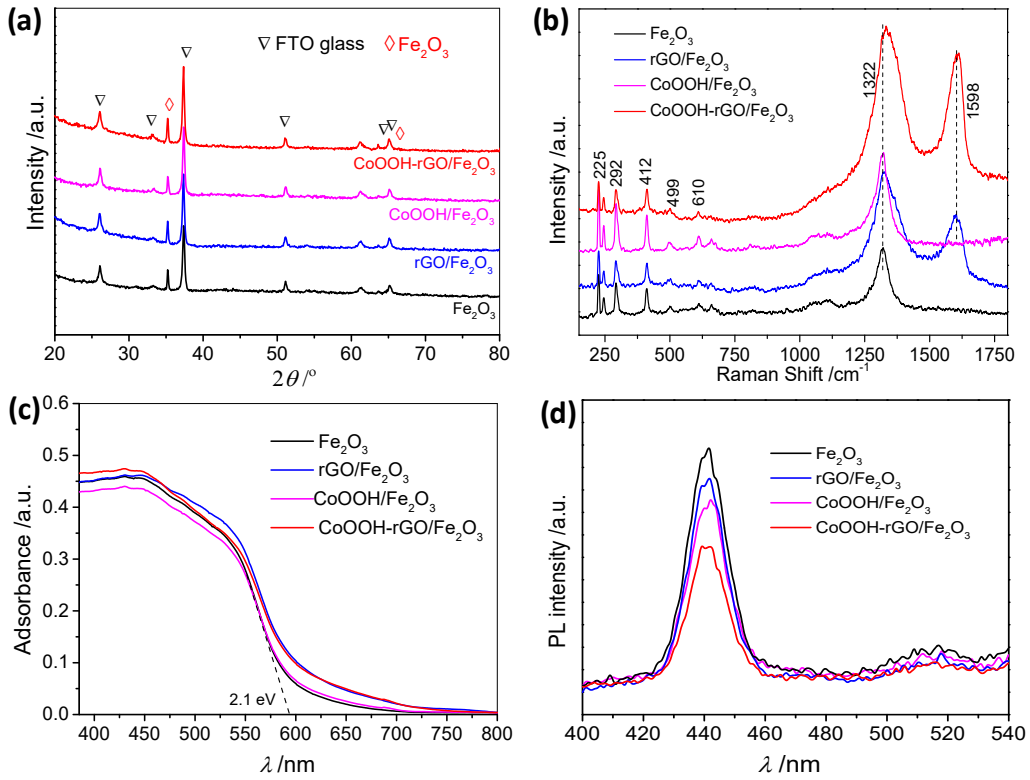

Figure 2 (a) XRD patterns, (b) Raman spectra, (c) UV-vis and (d) PL spectra of Fe_2O_3, rGO/Fe_2O_3, $CoOOH/Fe_2O_3$ and $CoOOH\text{-}rGO/Fe_2O_3$.

The crystalline phase and composition of the as-prepared samples were examined by XRD and Raman spectra. As seen in Figure 2a, all samples exhibit analogous XRD diffraction peaks. Among them, the peaks at 35.2° and 63.6° could be indexed to the (001) and (012) planes of α-phase Fe_2O_3, while the peaks at 26.1°, 33.1°, 37.4°, 51.1°, 61.1° and 65.1° are ascribed to SnO_2 in FTO glass. No other reflections related to rGO and CoOOH were observed, which might be attributed to the low loading amount. To further demonstrate the presence of rGO and CoOOH in these samples, Raman spectra were performed from 200~1800 cm^{-1}. As shown in Figure 2b, the peaks at 225 and 499 cm^{-1} are assigned to A1g vibrational mode, and those at 292, 412 and 610 cm^{-1} are

indexed to Eg mode, while the peak at 1322 cm^{-1} is assigned to the two magnon scattering, of Fe_2O_3.[51,52] With the decoration of rGO, a peak around 1598 cm^{-1}, which is the G band of rGO, is obviously observed, indicating the formation of rGO. While D band of rGO at 1340 cm^{-1} has not been clearly shown, which might be attributed to the overlap with the peak at 1322 cm^{-1} of Fe_2O_3. As a result, the full width at half maximum peak (FWHM) values around 1322 cm^{-1} for rGO/Fe_2O_3 and CoOOH-rGO/Fe_2O_3 are significantly larger than that of Fe_2O_3 and CoOOH/Fe_2O_3 (Figure S5). However, no characteristic vibrational modes of CoOOH at 499, 575 and 634 cm^{-1} were observed,[53] possibly owing to the weak vibrational intensity or the overlap with the vibrational modes of Fe_2O_3.

The optical properties of the samples were examined by UV-Vis diffuse reflectance (UV-vis DRS) and photoluminescence (PL) spectroscopies. The Fe_2O_3 exhibits an absorption edge at approximately 590 nm (Figure 2c), corresponding to the band gap of 2.1 eV. After the introduction of rGO and/or CoOOH onto Fe_2O_3, no significant difference was observed in UV-vis DRS, which suggests a negligible contribution to PEC performance caused by optical absorption. The PL emission, originating from the recombination of the separated electrons and holes, could reflect the separation, migration and transfer of photogenerated charges. As shown in Figure 2d, a strong emission peak around 440 nm for all samples could be attributed to the band-band PL phenomenon.[51,54] The strongest PL intensity for Fe_2O_3 indicates serious charge recombination occurs in Fe_2O_3. The PL intensity decreases obviously after the decoration with rGO or CoOOH onto Fe_2O_3, and further declines in CoOOH-

rGO/Fe_2O_3. The decreased PL intensity reveals the suppressed recombination of electrons and holes in the samples. The weakest PL intensity of CoOOH-rGO/Fe_2O_3 indicates both CoOOH and rGO can greatly benefits the separation of electron-hole pairs.[55]

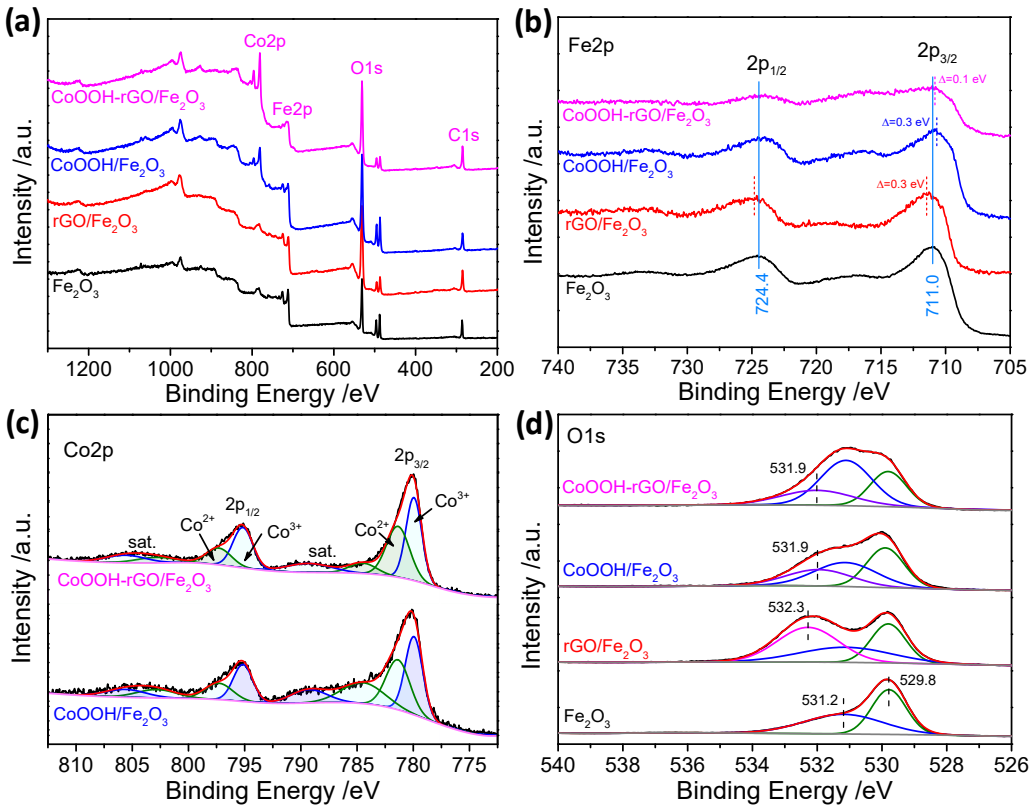

Figure 3 (a) The survey spectra, (b) Fe 2p, (c) Co 2p and (d) O 1s of Fe_2O_3, rGO/Fe_2O_3, CoOOH/Fe_2O_3 and CoOOH-rGO/Fe_2O_3.

To determine the chemical states of CoOOH on the surface of the samples, X-ray photoelectron spectroscopy (XPS) was carried out. The survey spectra identify the presence of Fe, Co, O and C species in corresponding sample (Figure 3a). The Fe 2p XPS spectra shows two major peaks at 711.0 ($2p_{3/2}$) and 724.4 eV ($2p_{1/2}$), matching well with the characteristic Fe(III) in Fe_2O_3 (Figure 3b). The binding energy of Fe 2p for rGO/Fe_2O_3 shows a slightly positive shift of *ca.* 0.3 eV, indicating an intimate

interaction between rGO and Fe_2O_3, which will facilitate charge transfer in the composite electrode.[39,49,56] In contrast, the binding energy of Fe 2p in CoOOH/Fe_2O_3 is detected with slight negative-shift compared with Fe_2O_3, indicating charge transfer from CoOOH to Fe_2O_3. After combined with rGO and CoOOH, Fe 2p peaks shift close to the position of that in Fe_2O_3, suggesting a reversed effect of rGO and CoOOH toward Fe_2O_3. This effect would be beneficial for the migration of photogenerated charges in different directions. Figure 3c shows the similarity of Co 2p core-level spectra for CoOOH/Fe_2O_3 and CoOOH-rGO/Fe_2O_3, indicating the same states of Co species existing in the samples. The further deconvolution for Co 2p spectra exhibits the binding energies at 780.0 and 795.2 eV for Co^{3+} 2p3/2 and 2p1/2 respectively. The binding energies at 781.5 and 797.5 eV for Co^{2+} 2p3/2 and 2p1/2 respectively. The results suggest the coexistence of Co^{3+} and Co^{2+} species in CoOOH. [47,57,58] Of note, the peak intensity for Co^{3+} is obviously stronger than that of Co^{2+}, indicating Co species dominates +3 oxidation state. The O 1s spectra show clear variation with various samples (Figure 3d). For bare Fe_2O_3, two peaks can be well fitted at the binding energy of 529.8 and 531.2 eV, corresponding to the lattice O (Fe-O) and the lattice hydroxyl group (Fe-OH). The O 1s for rGO/Fe_2O_3 shows three peaks at 529.8, 531.2 and 532.3 eV, matching well with the lattice O (Fe-O), the lattice hydroxyl group (Fe-OH) and the O in adsorbed water accordingly. While O1s spectra for both CoOOH/Fe_2O_3 and CoOOH-rGO/Fe_2O_3 were deconvoluted into three peaks at 529.8, 531.2 and 531.9 eV, which could be assigned the lattice O (Fe-O, Co-O), lattice hydroxyl group (Fe-OH, Co-OH) and the adsorbed hydroxyl group (OH^-) from the

hydrolysis process. The C 1s for all samples were deconvoluted at the binding energies of 284.8, 286.5 and 288.2 eV, corresponding to the C species in C-C with the sp^2 orbital, C-O and C=O respectively (Figure S6).[47,57,58] The C species in Fe_2O_3 and CoOOH/Fe_2O_3 might originate from the residual C or the absorbed C during the fabrication process or exposure to ambient. It is note that, the intensities for both C-O and C=O are almost negligible comparing with that of C-C in rGO/Fe_2O_3 and CoOOH-rGO/Fe_2O_3, indicating GO has been completely reduced to rGO under the designed experimental conditions.[38]

PEC water oxidation performance for Fe_2O_3, rGO/Fe_2O_3, CoOOH/Fe_2O_3 and CoOOH-rGO/Fe_2O_3 were first examined by linear sweep voltammetry (LSV) method (Figure 4a). The bare Fe_2O_3 exhibits a relatively low photoresponse over the entire potential window, with a photocurrent density (*J*) of *ca.* 0.78 mA cm^{-2} at 1.23 V *vs*. RHE. Both rGO/Fe_2O_3 and CoOOH/Fe_2O_3 show obviously enhanced photocurrent densities in whole potential range, with 1.29 mA cm^{-2} and 2.06 mA cm^{-2} at 1.23 V *vs*. RHE, respectively. The CoOOH-rGO/Fe_2O_3 shows the best PEC performance with the photocurrent density of 2.57 mA cm^{-2} at 1.23 V *vs*. RHE, suggesting a synergistic effect of rGO and CoOOH in PEC process. The onset potentials for water oxidation were further analyzed with Butler method.[11] CoOOH/Fe_2O_3 and CoOOH-rGO/Fe_2O_3 show a cathodic shift of onset potential by *ca.* 150 mV from 0.81 V to 0.66 V, compared with that of Fe_2O_3 and rGO/Fe_2O_3(Figure 4b). This result indicates the modification with CoOOH could reduce the energy barrier of water oxidation on Fe_2O_3 and thus facilitate the water oxidation kinetics. The similar cathodic shift of the onset potential

of water oxidation in the dark also demonstrates the positively catalytic effect of CoOOH (Figure S7). The photoresponse for the four photoanodes was also examined by the transient photocurrent measurement under chopped light irradiation (Figure 4c). As seen, all photoanodes sharply respond to the light on/off. Moreover, it also indicates the photocurrent occurs at much lower applied potential on CoOOH/Fe_2O_3 and CoOOH-rGO/Fe_2O_3, further demonstrating the efficiency of CoOOH decoration for water oxidation. The applied bias photon-to-current conversion efficiency (ABPE) for each photoanode was calculated below thermodynamic potential of water oxidation (*i.e.*, 1.23 V *vs*. RHE). As shown in Figure 4d, ABPE for CoOOH-rGO/Fe_2O_3 exhibits a maximum value (0.30%) at 0.99 V, which is slightly larger than that for CoOOH/Fe_2O_3 (0.28% at 0.97 V), but much larger than that for rGO/Fe_2O_3 (0.10% at 1.05 V) and Fe_2O_3 (0.08% at 1.04 V). The incident-photon-to-current conversion efficiency (IPCE) was further carried out to investigate the photo-response of each photoanode as a function of the irradiation wavelengths (Figure 4e). In the full wavelength range, IPCE values vary on photoanodes following the order of CoOOH-rGO/Fe_2O_3 > CoOOH/Fe_2O_3 > rGO/Fe_2O_3 > Fe_2O_3. The largest IPCE values shown by CoOOH-rGO/Fe_2O_3 in the all samples also confirm the synergistic effect of CoOOH and rGO on PEC performance. The long-term PEC performances of the photoanodes were measured by chronoamperometric *i-t* curves at 1.23 V *vs*. RHE under illumination (Figure 4f). No decrease in current density was observed in 2-hour test on the all photoanodes, indicating the species bound on the surface of Fe_2O_3 are photoelectrochemically stable.

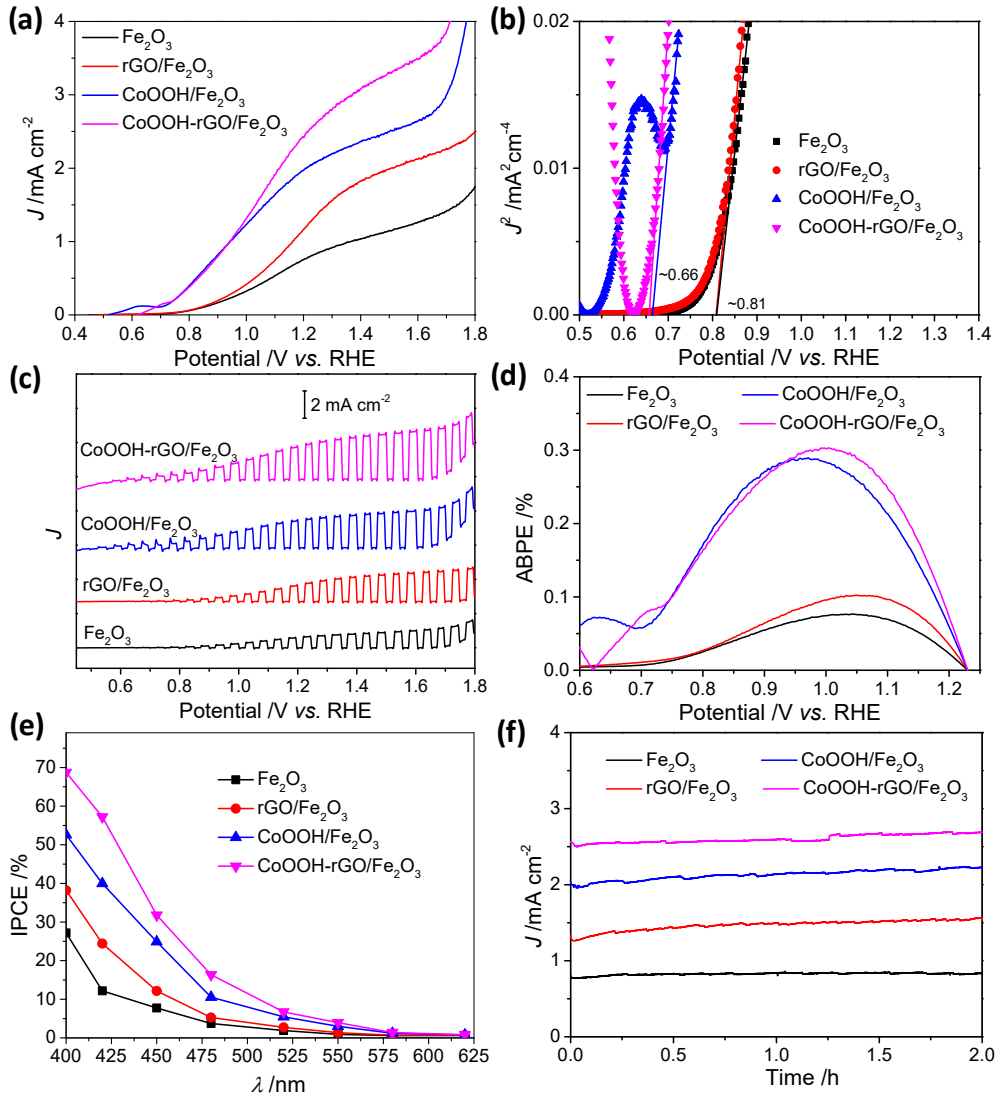

Figure 4 (a) LSV curves, (b) Butler plots, (c) LSV curves under chopped light, (d) ABPE curves, (e) IPCE curves and (f) *i-t* curves of Fe_2O_3, rGO/Fe_2O_3, $CoOOH/Fe_2O_3$ and $CoOOH\text{-}rGO/Fe_2O_3$.

The charge separation efficiency (η_{sep}) and the surface charge injection efficiency (η_{inj}) were examined by the comparison of photocurrent density in the absence/presence of SO_3^{2-} as a hole scavenger.[60,61] According to the standard solar spectrum and the

UV-vis absorption property of Fe_2O_3, the theoretical maximum photocurrent density (J_{abs}) was calculated to be 4.54 mA cm^{-2}, assuming 100% IPCE for incident photons (Figure S8).[60,61] Owing to negligible difference on UV-vis DRS for Fe_2O_3, rGO/Fe_2O_3, CoOOH/Fe_2O_3 and CoOOH-rGO/Fe_2O_3 (Figure 2c), the value of 4.54 mA cm^{-2} was used as J_{abs} to calculate the values of η_{sep} for all photoanodes. The photocurrent densities in the presence/absence of SO_3^{2-} are plotted in Figure S9 and the correspondingly calculated η_{sep} and η_{inj} are plotted as function of potential and displayed in Figures 5a and 5b. As shown in Figure 5a, a significantly promoted η_{sep} is observed in rGO/Fe_2O_3 (40.8% at 1.23 V) and CoOOH/Fe_2O_3 (48.2% at 1.23 V) compared with that of bare Fe_2O_3 (26.6% at 1.23 V). This result indicates the charge recombination is remarkably inhibited via the decoration of rGO or CoOOH on Fe_2O_3. Again, the largest η_{sep} of 55.4% at 1.23 V exhibited by CoOOH-rGO/Fe_2O_3 in these samples suggests a synergistic effect of CoOOH and rGO on the charge separation in Fe_2O_3. As clearly seen for η_{inj} from Figure 5b, the two photoelectrodes modified with CoOOH exhibit much higher values than the other two without CoOOH. This indicates CoOOH plays a greatly important role in enhancing the charge transfer from electrode surface to electrolyte. It is noted that, compared with rGO/Fe_2O_3, Fe_2O_3 photoelectrode showed a higher η_{inj} value in the low potential range (0.8~1.2 V) but a lower value in the high potential range (>1.2 V). This might be attributed to the surface defects which could also act as active centers for PEC water oxidation, even though they can act as recombination centers for photogenerated charges. All above observations clearly indicate that rGO can facilitate the charge separation and CoOOH not only can do so

but also can enhance the charge transfer.

The charge transfer behavior was further examined by electrochemical impedance spectroscopy (EIS). As shown in Figure 5c, Nyquist plots for all photoanodes demonstrate two semicircles, which can be assigned to the internal charge transfer resistances in the bulk of photoanode (R_{bulk}) and at the interface of photoanode/electrolyte (R_{trap}).[62,63] The smaller diameters of R_{bulk} and R_{trap} suggest a fast charge transfer in the bulk and at the surface of the photoanode, respectively.[63,64] Both parameters were evaluated by fitting the Nyquist plots with the equivalent circuit model (the inset in Figure 5c), in which R_s is the series resistances in the electrochemical cell, C_{trap} and C_{bulk} are the capacitance at the surface and in the depletion layer of the photoanode, respectively. As shown in Table S1, R_{bulk} values for the photoanodes with rGO (79.7Ω for CoOOH-rGO/Fe_2O_3 and 103.8Ω for rGO/Fe_2O_3) are significantly smaller than that for the others without rGO (197.2Ω for CoOOH/Fe_2O_3 and 221.5Ω for Fe_2O_3). This clearly indicates rGO could improve the bulk electrical conductivity of the photoanode. In addition, R_{trap} values for the photoanodes with CoOOH (471.1Ω for CoOOH-rGO/Fe_2O_3 and 629.5Ω for CoOOH/Fe_2O_3) are much smaller than that of the others without CoOOH (2117Ω for rGO/Fe_2O_3 and 2588Ω for Fe_2O_3). This result suggests CoOOH helps to enhance the charge transfer at the photoanode/electrolyte interface. The results are in line with the above analyses on η_{sep} and η_{inj}. To gain further insights into the impacts of CoOOH and rGO on charge behavior, Mott-Schottky (M-S) experiments for the samples were performed (Figure 5d). The flat band potential (*ca.* 0.62 V) of Fe_2O_3 and/or rGO/Fe_2O_3 is cathodically shifted to *ca.* 0.47 V for

CoOOH/Fe_2O_3 and/or CoOOH/rGO/Fe_2O_3. This cathodic shift is probably due to the efficient hole transfer from the bulk of Fe_2O_3 to its supported CoOOH, promoting the surface water oxidation reaction.[9,65] This result might be attributed to the reduction of Fermi level pinning effect caused by the surface state change of Fe_2O_3 after the decoration of CoOOH. Furthermore, the carrier densities (N_d) calculated from the slopes of M-S plots are 1.70×10^{19}, 2.80×10^{19}, 8.82×10^{19} and 9.97×10^{19} cm^{-3} for Fe_2O_3, rGO/Fe_2O_3, CoOOH/Fe_2O_3 and CoOOH-rGO/Fe_2O_3, respectively (Table S2). The remarkably increased N_d indicates CoOOH plays much more effective roles for carrier separation and thus improve the electrical conductivity and enhance PEC water oxidation.

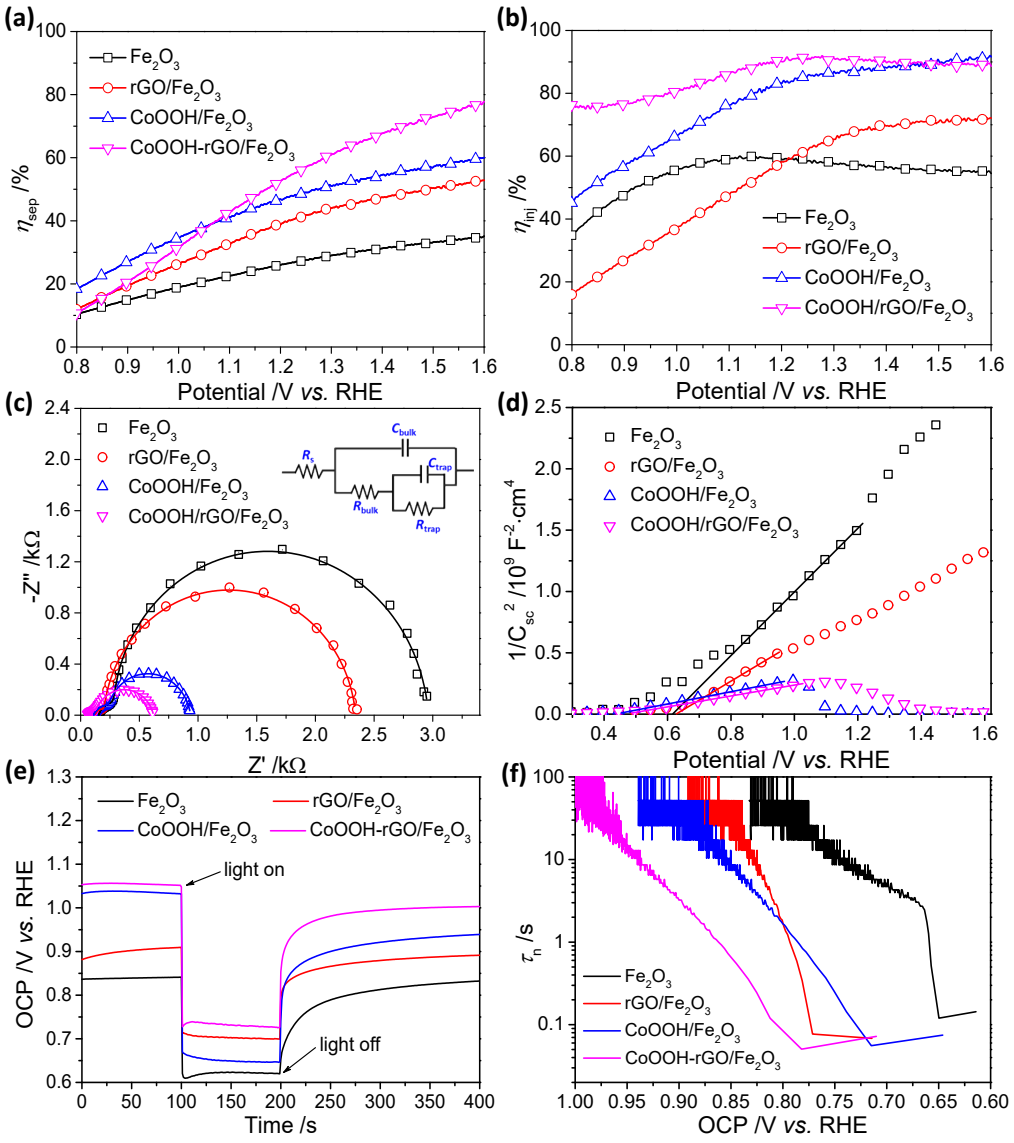

Figure 5 (a) The charge separation efficiency (η_{sep}), (b) the charge injection efficiency (η_{inj}), (c) Nyquist plots, (d) Mott-Schottky (M-S) curves, (e) OCP profiles under illumination and in dark and (f) potential dependent carrier lifetime for Fe_2O_3, rGO/Fe_2O_3, $CoOOH/Fe_2O_3$ and $CoOOH\text{-}rGO/Fe_2O_3$. The inset of (c) shows the equivalent circuit for EIS fitting.

To investigate the kinetics of charge transfer in the photoanodes, the dark/light open circuit potentials (OCPs) were measured. Figure 5e shows the potentials for all samples cathodically shift once the light is on, in accord with the characteristic of n-type

semiconductors.[66] The OCP value for Fe_2O_3 in darkness is at 0.84 V *vs.* RHE, while that for rGO/Fe_2O_3, CoOOH/Fe_2O_3 and CoOOH-rGO/Fe_2O_3 positively shift to 0.91, 1.03 and 1.05 V, indicating the elimination effects of rGO and CoOOH on the surface states of Fe_2O_3.[67] Figure S10 shows the difference of OCP before and after illumination ($\Delta OCP=OCP_{dark}-OCP_{light}$) on these samples. It is obvious that CoOOH/Fe_2O_3 and CoOOH-rGO/Fe_2O_3 have larger ΔOCP, compared with that of Fe_2O_3 and rGO/Fe_2O_3. In other words, CoOOH/Fe_2O_3 and CoOOH-rGO/Fe_2O_3 show higher photovoltages than Fe_2O_3 and rGO/Fe_2O_3, implying an increased band bending at the interface of CoOOH/Fe_2O_3 and CoOOH-rGO/Fe_2O_3 photoelectrodes with electrolyte. This means that CoOOH significantly promote the kinetics of charge separation and transfer at the interface of electrode and electrolyte.[61,66,68] To further illustrate the enhanced charger transfer kinetics, the lifetime of the generated charges (τ_n) after the light off as a function of OCP is calculated. As shown in Figure 5f, the charge lifetime shows in the order of CoOOH-rGO/Fe_2O_3 $\approx$ CoOOH/Fe_2O_3 < rGO/Fe_2O_3 < Fe_2O_3, which further indicates the faster charge transfer in CoOOH-rGO/Fe_2O_3 and CoOOH/Fe_2O_3 photoelectrodes.

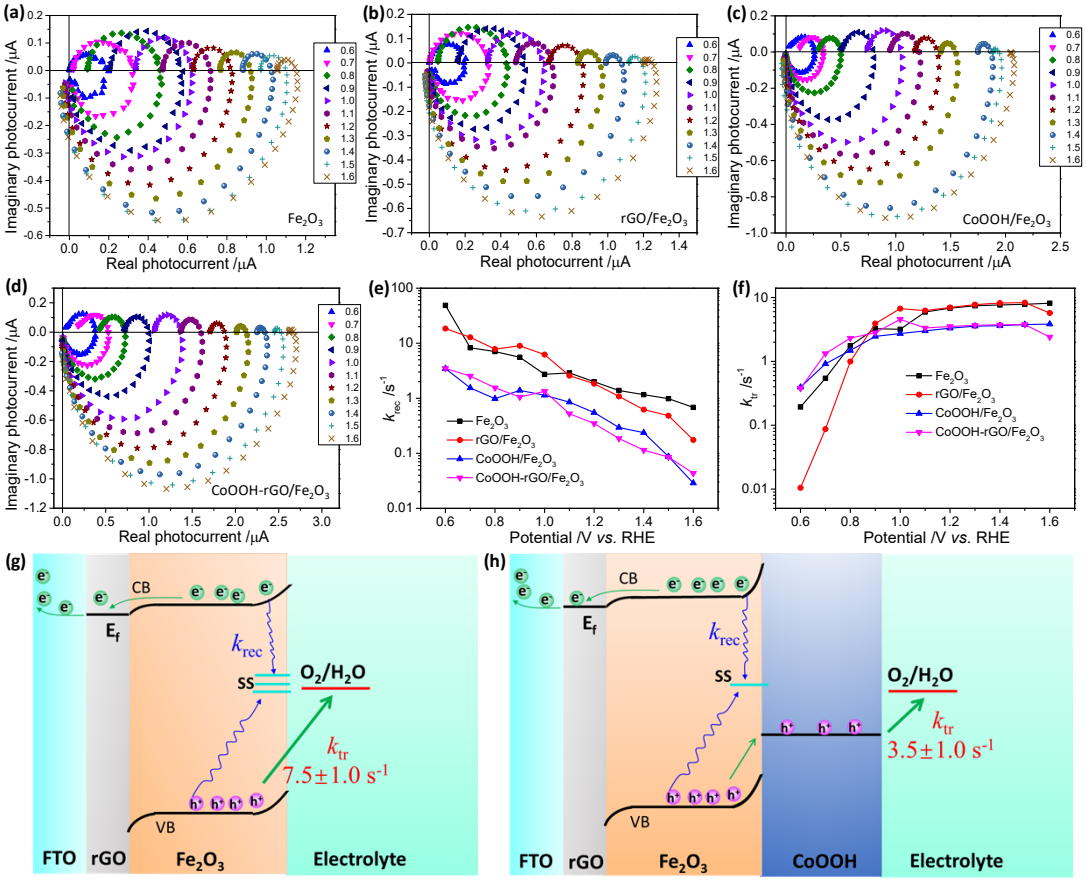

Figure 6 IMPS spectra of (a) Fe_2O_3, (b) rGO/Fe_2O_3, (c) CoOOH/Fe_2O_3 and (d) CoOOH-rGO/Fe_2O_3 under different applied potentials; (e) the surface charge recombination (k_{rec}) rate constants, (f) the surface charge transfer (k_{tr}) rate constants for Fe_2O_3, rGO/Fe_2O_3, CoOOH/Fe_2O_3 and CoOOH/rGO/Fe_2O_3; and, A representation for the holes transfer rates at 1.2 V *vs.* RHE over (g) Fe_2O_3 and (h) CoOOH/rGO/Fe_2O_3 via different pathways.

In order to understand how rGO or CoOOH improves PEC water oxidation, the kinetics of charge transfer and recombination on the surface of these samples were quantified by intensity modulated photocurrent spectroscopy (IMPS) in the potential range of 0.6 to 1.6 V *vs.* RHE (Figure 6a-d). All IMPS plots are shown with two

semicircles character (Figure S11). The first semicircle in the 4th quadrant is related to the charge transfer process in the bulk (that is, the transient time of the electron, τ_d) and determined by the *RC* time constant of the photoelectrode in the high frequency range. The second semicircle in the 1st quadrant is related to the balance between the charge recombination (k_{rec}) and the charge transfer (k_{tr}) on the surface.[69] The analysis of IMPS thus gives the values of τ_d, k_{rec} and k_{tr}.[70-72] Figure S12 shows the τ_d values are roughly in the order of Fe_2O_3 (0.148 ms) < rGO/Fe_2O_3 ≈ CoOOH-rGO/Fe_2O_3 (0.196-0.260 ms) < CoOOH/Fe_2O_3 (0.453 ms). This phenomenon might be related to the migration pathway of the photogenerated electrons on the photoelectrode. The Fe_2O_3 photoelectrode showed the lowest value of τ_d in all samples. We speculate that only electrons which are close to the FTO substrate can be captured and those far away from the FTO will be recombined during the long-distance migration (Scheme S1a) in Fe_2O_3 photoelectrode. On the contrary, the effective electrons for CoOOH/Fe_2O_3 might come from the distant region (Scheme S1b), like the terminal of Fe_2O_3 nanorods, owing to the typical tree-like structure of CoOOH/Fe_2O_3. As for rGO/Fe_2O_3, the larger τ_d of rGO/Fe_2O_3 would be attributed to the transient retention of electrons on rGO (Scheme S1c). The smaller τ_d of CoOOH-rGO/Fe_2O_3 than that of CoOOH/Fe_2O_3, with the comparable τ_d of rGO/Fe_2O_3, suggesting rGO plays an important role that modulate the migration of electrons from Fe_2O_3 nanorods to FTO substrate (Scheme S1d).[70-72]

Figure 6e shows the surface recombination rate constants (k_{rec}) at different potentials. The similar k_{rec} values for rGO/Fe_2O_3 with that for bare Fe_2O_3 indicate the surface passivation caused by rGO is slight. In contrast, k_{rec} values for CoOOH/Fe_2O_3 and

CoOOH-rGO/Fe_2O_3 are significantly lower than that of bare Fe_2O_3 and rGO/Fe_2O_3, suggesting CoOOH causes much more powerful passivation of the surface states of Fe_2O_3. The comparison of charge transfer rate constants (k_{tr}) seems much more complicated than that of k_{rec} and two potential regions can be distinguished for the samples (Figure 6f). For potentials lower than 0.9 V *vs.* RHE, k_{tr} shows the order of rGO/Fe_2O_3 < Fe_2O_3 < CoOOH/Fe_2O_3 ≈ CoOOH-rGO/Fe_2O_3, clearly indicating the enhanced charge transfer promoted by CoOOH. Conversely, for bias at higher than 0.9 V *vs.* RHE, rGO/Fe_2O_3 and Fe_2O_3 photoanode yield comparable even higher k_{tr} values than that of CoOOH/Fe_2O_3 and CoOOH-rGO/Fe_2O_3. For instance, k_{tr} value is 7.5±1.0 s^{-1} for Fe_2O_3 and rGO/Fe_2O_3 at 1.2 V *vs.* RHE, which is higher than these of CoOOH/Fe_2O_3 and CoOOH-rGO/Fe_2O_3 (3.5±0.5 s^{-1}). This result might be owing to the instinct stronger thermodynamic driving force of the holes on valence band of Fe_2O_3 (2.48 V *vs*. RHE) than that of Co^{3+}/Co^{2+} redox potentials (1.55 V *vs*. RHE).[75] A representation is schematically shown in Figures 6g and 6h to understand the hole transfer rates over Fe_2O_3/electrolyte and Fe_2O_3/CoOOH/electrolyte interface at higher potential of 1.2. Although Fe_2O_3 and rGO/Fe_2O_3 have a higher k_{tr} value than CoOOH/Fe_2O_3 and CoOOH-rGO/Fe_2O_3, their large k_{rec} values finally results in low PEC activity (the trend of the photocurrents in Figure 4a).

Based on the above discussions, a mechanism of rGO and CoOOH jointly boosting PEC water oxidation is proposed. Due to the instinct poor conductivity, short hole diffusion length and rich surface states, Fe_2O_3 shows poor electron transfer and serious recombination in the bulk and at the surface (Scheme 2a) [5]. With the incorporation of

rGO, the photogenerated electrons in Fe_2O_3 are induced to drift into network owing to the binding energy alignment between rGO and Fe_2O_3.[38,39] Therefore, the lifetime of these localized electrons is prolonged, corresponding to the suppressed charge recombination and the slightly enhanced charge separation. The decoration of CoOOH leads to the reduced surface states and the increased band bending at the interface of photoelectrode/electrolyte, thus the photogenerated holes would easily migrate to CoOOH and subsequently the surface recombination is reduced (Figure S15b). With the decoration of rGO combined with CoOOH, the electron transfer was improved, as well as the bulk and the surface recombination were significantly suppressed (Scheme 2b). And ultimately, CoOOH-rGO/Fe_2O_3 exhibits significantly boosted PEC water oxidation performance, compared with that of Fe_2O_3. It should be noted that, even though k_{tr} over CoOOH-rGO/Fe_2O_3 is comparably lower than that of Fe_2O_3, the combined effect from the improved electron transfer, the enhanced bulk charge separation and the significantly suppressed surface recombination still makes CoOOH-rGO/Fe_2O_3 possess much more excellent PEC activity.

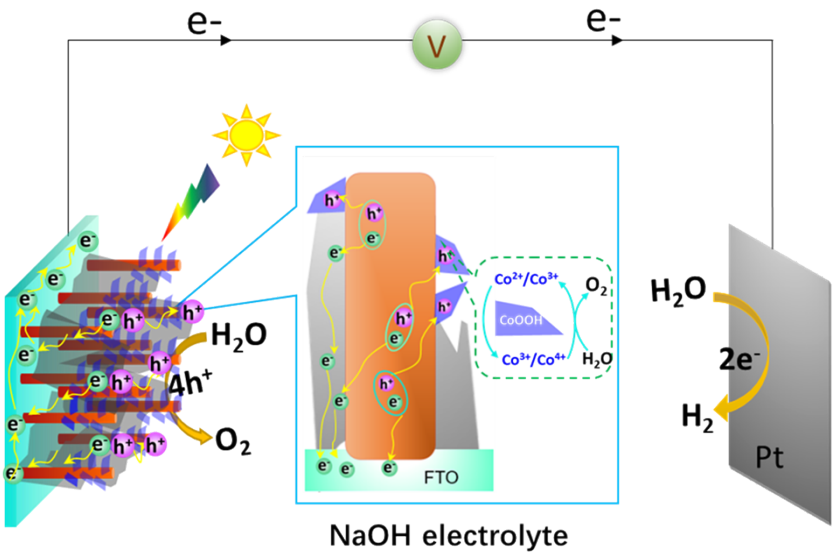

Scheme 2 Charge transfer mechanism in CoOOH-rGO/Fe_2O_3 photoanode.

Furthermore, a plausible water oxidation mechanism occurring at CoOOH-rGO/Fe_2O_3 electrode for boosted PEC water oxidation is elucidated in Scheme 3. Under illumination, Fe_2O_3 generates electron-hole (e_-h+) pairs, which are subsequently separated to electrons and holes. The photogenerated electrons are then transferred to FTO substrate easily via the conductive rGO network, and ultimately to Pt counter electrode for H_2 generation. Meanwhile, the photogenerated holes (h^+) are transferred to CoOOH, in which $C^{o2}+/Co^{3+}$ species trap holes to form Co^{3+}/Co^{4+} species [30]. Subsequently Co^{3+}/Co^{4+} act as active sites for water oxidation to produce oxygen (O2). It is thus believed that the significant enhancement in PEC performance of CoOOH-rGO/Fe_2O_3 is ascribed to the improved electron migration, enhanced charge separation, efficient holes capture and transfer, and significantly suppressed surface recombination caused by spatially separated CoOOH and rGO.

3 Conclusion

A facile hydrothermal process combining with a chelation-mediated in-situ growth route was developed to fabricate spatially separated rGO and CoOOH co-incorporated Fe_2O_3 photoanode. The as-prepared CoOOH-rGO/Fe_2O_3 achieves a remarkably enhanced photocurrent density of *ca.* 2.57 mA cm^{-2} at 1.23 V *vs.* RHE in alkaline electrolyte, significantly higher than that of CoOOH/Fe_2O_3, rGO/Fe_2O_3 and Fe_2O_3. The enhanced PEC performance for CoOOH-rGO/Fe_2O_3 is attributed to the synergistic effect of CoOOH and rGO: the rGO serves as electron transfer channel to accelerate the electron transfer from Fe_2O_3 to FTO substrate, and CoOOH as oxygen evolution

cocatalysts enhances the charge separation ~~and the holes transfer~~. The kinetics study of charge transfer on the surface of CoOOH-rGO/Fe_2O_3 by IMPS suggests that the effect of CoOOH on promoting charge separation in Fe_2O_3 is more pronounced than that on enhancing holes transfer from Fe_2O_3 to the electrolyte. The suppression of the charge recombination and the electron transfer are demonstrated as two key factors to improve toward making highly efficient Fe_2O_3 photoelectrodes. This synthesis strategy of co-incorporating rGO and CoOOH can be used for other analogous photoanodes, such as TiO_2, WO_3, $BiVO_4$ *etc.*, to achieve highly efficient PEC systems.

Supporting Information

Supporting Information is available from the Wiley Online Library or from the author.

Conflict of Interest

The authors declare no conflict of interest.

Acknowledgements

The work was supported by the National Natural Science Foundation of China (U2004195 and 51502078), the Foundation for University Youth Key Teachers from Henan Province (2020GGJS036), the Major Project of Science and Technology, Education Department of Henan Province (19A150019 and 19A150018), the Science and Technology Research Project of Henan Province (192102310490 and 182102410090), the program for Science & Technology Innovation Team in Universities of Henan Province (19IRTSTHN029). X.W. was supported by the U.S. Department of Energy, Office of Science, Office of Basic Energy Sciences, Chemical

Sciences, Geosciences, and Biosciences Division, Catalysis Science program.

References

[1] A. Fujishima, K. Honda, Electrochemical Photolysis of Water at a Semiconductor Electrode, Nature (1972) 37-38.

[2] G. Zheng, J. Wang, H. Liu, V. Murugadoss, G. Zu, H. Che, C. Lai, H. Li, T. Ding, Q. Gao, Z. Guo, O.R.T.U. Oak Ridge National Lab. Ornl, Tungsten Oxide Nanostructures and Nanocomposites for Photoelectrochemical Water Splitting, Nanoscale 11 (2019) 18968-18994.

[3] C. Li, Z. Luo, T. Wang, J. Gong, Surface, Bulk, and Interface: Rational Design of Hematite Architecture Toward Efficient Photo-Electrochemical Water Splitting, Advanced materials (Weinheim) 30 (2018) 1707502.

[4] J.H. Kim, J.S. Lee, Elaborately Modified $Bivo_4$ Photoanodes for Solar Water Splitting, Adv. Mater. 31 (2019) n/a-n/a.

[5] S. Shen, S.A. Lindley, X. Chen, J.Z. Zhang, Hematite Heterostructures for Photoelectrochemical Water Splitting: Rational Materials Design and Charge Carrier Dynamics, Energ. Environ. Sci. 9 (2016) 2744-2775.

[6] P. Sharma, J. Jang, J.S. Lee, Key Strategies to Advance the Photoelectrochemical Water Splitting Performance of A -Fe_2O_3 Photoanode, Chemcatchem 11 (2019) 157.

[7] K.C. Bedin, D.N.F. Muche, M.A. Melo, A.L.M. Freitas, R.V. Gonçalves, F.L. Souza, Role of Cocatalysts On Hematite Photoanodes in Photoelectrocatalytic Water Splitting: Challenges and Future Perspectives, Chemcatchem 12 (2020) 3156-3169.

[8] F. Li, J. Li, J. Zhang, L. Gao, X. Long, Y. Hu, S. Li, J. Jin, J. Ma, Nio Nanoparticles Anchored

On Phosphorus-Doped A -Fe_2O_3 Nanoarrays: An Efficient Hole Extraction P-N Heterojunction Photoanode for Water Oxidation, Chemsuschem 11 (2018) 2156-2164.

[9] S. Yi, B. Wulan, J. Yan, Q. Jiang, Highly Efficient Photoelectrochemical Water Splitting: Surface Modification of Cobalt-Phosphate-Loaded Co_3O_4/Fe_2O_3 P-N Heterojunction Nanorod Arrays, Adv. Funct. Mater. 29 (2019)

[10] P. Zhang, T. Wang, X. Chang, L. Zhang, J. Gong, Synergistic Cocatalytic Effect of Carbon Nanodots and Co_3O_4 Nanoclusters for the Photoelectrochemical Water Oxidation On Hematite, Angew. Chem. Int. Edit. 55 (2016) 5851-5855.

[11] C. Du, X. Yang, M.T. Mayer, H. Hoyt, J. Xie, G. Mcmahon, G. Bischoping, D. Wang, Hematite-Based Water Splitting with Low Turn-On Voltages, Angew. Chem. Int. Edit. 52 (2013) 12692-12695.

[12] Y. Xu, X. Wang, H. Chen, D. Kuang, C. Su, Toward High Performance Photoelectrochemical Water Oxidation: Combined Effects of Ultrafine Cobalt Iron Oxide Nanoparticle, Adv. Funct. Mater. 26 (2016) 4414-4421.

[13] W. Ma, X. Wu, K. Huang, M. Wang, R. Fu, H. Chen, S. Feng, A $Co(Oh)_X$ Nanolayer Integrated Planar Wo_3/Fe_2O_3 Photoanode for Efficient Photoelectrochemical Water Splitting, SUSTAINABLE ENERGY & FUELS 3 (2019) 2135-2141.

[14] Q. Liu, F. Cao, F. Wu, H. Lu, L. Li, Ultrathin Amorphous $Ni(Oh)_2$ Nanosheets On Ultrathin A -Fe_2O_3 Films for Improved Photoelectrochemical Water Oxidation, ADVANCED MATERIALS INTERFACES 3 (2016)

[15] G. Wang, Y. Ling, X. Lu, T. Zhai, F. Qian, Y. Tong, Y. Li, A Mechanistic Study Into the Catalytic Effect of $Ni(Oh)_2$ On Hematite for Photoelectrochemical Water Oxidation,

Nanoscale 5 (2013) 4129-4133.

[16] M. Li, T. Liu, Y. Yang, W. Qiu, C. Liang, Y. Tong, Y. Li, Zipping Up Nife$(Oh)_X$-Encapsulated Hematite to Achieve an Ultralow Turn-On Potential for Water Oxidation, ACS ENERGY LETTERS 4 (2019) 1983-1990.

[17] F. Malara, A. Minguzzi, M. Marelli, S. Morandi, R. Psaro, V. Dal Santo, A. Naldoni, α-Fe_2O_3/Niooh: An Effective Heterostructure for Photoelectrochemical Water Oxidation, Acs Catal. 5 (2015) 5292-5300.

[18] A.G. Tamirat, W. Su, A.A. Dubale, H. Chen, B. Hwang, Photoelectrochemical Water Splitting at Low Applied Potential Using a Niooh Coated Codoped (Sn, Zr) α-Fe_2O_3 Photoanode, J. Mater. Chem. A 3 (2015) 5949-5961.

[19] K. Ye, Z. Wang, H. Li, Y. Yuan, Y. Huang, W. Mai, A Novel Coooh/(Ti, C)-Fe_2O_3 Nanorod Photoanode for Photoelectrochemical Water Splitting, SCIENCE CHINA-MATERIALS 61 (2018) 887-894.

[20] C. Liu, Y. Xu, H. Luo, W. Wang, Q. Liang, Z. Chen, Synthesis and Photoelectrochemical Properties of Coooh/Phosphorus-Doped Hematite Photoanodes for Solar Water Oxidation, Chem. Eng. J. 363 (2019) 23-32.

[21] D. Chen, Z. Liu, S. Zhang, Enhanced Pec Performance of Hematite Photoanode Coupled with Bimetallic Oxyhydroxide Nifeooh through a Simple Electroless Method, Appl. Catal. B-Environ. 265 (2020)

[22] M. Barroso, A.J. Cowan, S.R. Pendlebury, M. Graetzel, D.R. Klug, J.R. Durrant, The Role of Cobalt Phosphate in Enhancing the Photocatalytic Activity of α-Fe_2O_3 Toward Water Oxidation, J. Am. Chem. Soc. 133 (2011) 14868-14871.

[23] R. Chong, B. Wang, D. Li, Z. Chang, L. Zhang, Enhanced Photoelectrochemical Activity of Nickel-Phosphate Decorated Phosphate-Fe_2O_3 Photoanode for Glycerol-Based Fuel Cell, Solar Energy Materials & Solar Cells 160 (2017) 287-293.

[24] G. Liu, Y. Zhao, K. Wang, D. He, R. Yao, J. Li, Ultrasmall Nife-Phosphate Nanoparticles Incorporated A - Fe_2O_3 Nanoarrays Photoanode Realizing High Efficient Solar Water Splitting, ACS Sustainable Chem. Eng. 6 (2018) 2353-2361.

[25] Q. Bu, S. Li, Q. Wu, Y. Lin, D. Wang, X. Zou, T. Xie, In Situ Synthesis of Fep-Decorated Ti-Fe_2O_3: An Effective Strategy to Improve the Interfacial Charge Transfer in the Photoelectrochemical Water Oxidation Reaction, Catal. Sci. Technol. 9 (2019) 5812-5818.

[26] S.C. Shit, I. Mondal, S. Pendem, L. Bai, J.Y. Park, J. Mondal, Mof-Derived Bifunctional Iron Oxide and Iron Phosphide Nanoarchitecture Photoelectrode for Neutral Water Splitting, CHEMELECTROCHEM 5 (2018) 2842-2849.

[27] Q. Bu, S. Li, S. Cao, Q. Zhao, Y. Chen, D. Wang, T. Xie, A Ni_2P Modified Ti^{4+} Doped Fe_2O_3 Photoanode for Efficient Solar Water Oxidation by Promoting Hole Injection, Dalton T. 46 (2017) 10549-10552.

[28] R. Chong, G. Wang, Y. Du, Y. Jia, X. Wang, C. Li, Z. Chang, L. Zhang, Anion Engineering of Exfoliated Coal Layered Double Hydroxides On Hematite Photoanode Toward Highly Efficient Photoelectrochemical Water Splitting, Chem. Eng. J. 366 (2019) 523-530.

[29] R. Chong, B. Wang, C. Su, D. Li, L. Mao, Z. Chang, L. Zhang, Dual-Functional Coal Layered Double Hydroxide Decorated A -Fe_2O_3 as an Efficient and Stable Photoanode for Photoelectrochemical Water Oxidation in Neutral Electrolyte, J. Mater. Chem. A 5 (2017) 8583-8590.

[30] C. Wang, X. Long, S. Wei, T. Wang, F. Li, L. Gao, Y. Hu, S. Li, J. Jin, Conformally Coupling Coal-Layered Double Hydroxides On Fluorine-Doped Hematite: Surface and Bulk Co-Modification for Enhanced Photoelectrochemical Water Oxidation, Acs Appl. Mater. Inter. 11 (2019) 29799-29806.

[31] G. Yang, Y. Li, H. Pang, K. Chang, J. Ye, Ultrathin Cobalt-Manganese Nanosheets: An Efficient Platform for Enhanced Photoelectrochemical Water Oxidation with Electron-Donating Effect, Adv. Funct. Mater. 29 (2019)

[32] H. Ahn, A. Goswami, F. Riboni, S. Kment, A. Naldoni, S. Mohajernia, R. Zboril, P. Schmuki, Hematite Photoanode with Complex Nanoarchitecture Providing Tunable Gradient Doping and Low Onset Potential for Photoelectrochemical Water Splitting, Chemsuschem 11 (2018) 1873-1879.

[33] Y.B. Park, J.H. Kim, Y.J. Jang, J.H. Lee, M.H. Lee, B.J. Lee, D.H. Youn, J.S. Lee, Exfoliated Nife Layered Double Hydroxide Cocatalyst for Enhanced Photoelectrochemical Water Oxidation with Hematite Photoanode, Chemcatchem 11 (2019) 443-448.

[34] Y. Zhu, X. Zhao, J. Li, H. Zhang, S. Chen, W. Han, D. Yang, Surface Modification of Hematite Photoanode by Nife Layered Double Hydroxide for Boosting Photoelectrocatalytic Water Oxidation, J. Alloy. Compd. 764 (2018) 341-346.

[35] G. Wang, B. Wang, C. Su, D. Li, L. Zhang, R. Chong, Z. Chang, Enhancing and Stabilizing A -Fe_2O_3 Photoanode Towards Neutral Water Oxidation: Introducing a Dual-Functional Nicoal Layered Double Hydroxide Overlayer, J. Catal. 359 (2018) 287-295.

[36] L. Wang, T.N. Nhat, Y. Zhang, Y. Bi, P. Schmuki, Enhanced Solar Water Splitting by Swift Charge Separation in Au/Feooh Sandwiched Single-Crystalline Fe_2O_3 Nanoflake

Photoelectrodes, Chemsuschem 10 (2017) 2720-2727.

[37] L. Wang, T.N. Nhat, X. Huang, P. Schmuki, Y. Bi, Hematite Photoanodes: Synergetic Enhancement of Light Harvesting and Charge Management by Sandwiched with Fe_2Tio_5/Fe_2O_3/Pt Structures, Adv. Funct. Mater. 27 (2017)

[38] F. Meng, J. Li, S.K. Cushing, J. Bright, M. Zhi, J.D. Rowley, Z. Hong, A. Manivannan, A.D. Bristow, N. Wu, Photocatalytic Water Oxidation by Hematite/Reduced Graphene Oxide Composites, Acs Catal. 3 (2013) 746-751.

[39] F. Ning, M. Shao, S. Xu, Y. Fu, R. Zhang, M. Wei, D.G. Evans, X. Duan, Tio_2/Graphene/Nife-Layered Double Hydroxide Nanorod Array Photoanodes for Efficient Photoelectrochemical Water Splitting, Energ. Environ. Sci. 9 (2016) 2633-2643.

[40] L. Sun, J. Sun, X. Yang, S. Bai, Y. Feng, R. Luo, D. Li, A. Chen, An Integrating Photoanode Consisting of $Bivo_4$, Rgo and Ldh for Photoelectrochemical Water Splitting, Dalton T. 48 (2019) 16091-16098.

[41] J. Zhou, Y. Wang, X. Su, S. Gu, R. Liu, Y. Huang, S. Yan, J. Li, S. Zhang, Electrochemically Accessing Ultrathin Co (Oxy)-Hydroxide Nanosheets and Operando Identifying their Active Phase for the Oxygen Evolution Reaction, Energ. Environ. Sci. 12 (2019) 739-746.

[42] M. Bajdich, M. Garcia-Mota, A. Vojvodic, J.K. Norskov, A.T. Bell, Theoretical Investigation of the Activity of Cobalt Oxides for the Electrochemical Oxidation of Water, J. Am. Chem. Soc. 135 (2013) 13521-13530.

[43] B. Zhang, X. Zheng, O. Voznyy, R. Comin, M. Bajdich, M. Garcia-Melchor, L. Han, J. Xu, M. Liu, L. Zheng, F.P.G. de Arquer, C.T. Dinh, F. Fan, M. Yuan, E. Yassitepe, N. Chen, T. Regier, P. Liu, Y. Li, P. De Luna, A. Janmohamed, H.L. Xin, H. Yang, A. Vojvodic, E.H. Sargent,

Homogeneously Dispersed Multimetal Oxygen-Evolving Catalysts, Science 352 (2016) 333-337.

[44] U. Maitra, B.S. Naidu, A. Govindaraj, C.N.R. Rao, Importance of Trivalency and the E_{g1} Configuration in the Photocatalytic Oxidation of Water by Mn and Co Oxides, P. Natl. Acad. Sci. Usa. 110 (2013) 11704-11707.

[45] J. Suntivich, K.J. May, H.A. Gasteiger, J.B. Goodenough, Y. Shao-Horn, A Perovskite Oxide Optimized for Oxygen Evolution Catalysis From Molecular Orbital Principles, Science 334 (2011) 1383-1385.

[46] F. Tang, W. Cheng, H. Su, X. Zhao, Q. Liu, Smoothing Surface Trapping States in 3D Coral-Like Coooh-Wrapped-$Bivo_4$ for Efficient Photoelectrochemical Water Oxidation, Acs Appl. Mater. Inter. 10 (2018) 6228-6234.

[47] B. Zhang, X. Huang, H. Hu, L. Chou, Y. Bi, Defect-Rich and Ultrathin Coooh Nanolayers as Highly Efficient Oxygen Evolution Catalysts for Photoelectrochemical Water Splitting, J. Mater. Chem. A 7 (2019) 4415-4419.

[48] Z. Wang, J. Rong, J. Lv, R. Chong, L. Zhang, L. Wang, Z. Chang, X. Wang, Chelation-Mediated in-Situ Formation of Ultrathin Cobalt (Oxy)Hydroxides On Hematite Photoanode Towards Enhanced Photoelectrochemical Water Oxidation, J. Energy Chem. 56 (2021) 152-161.

[49] R. Boppella, C.H. Choi, J. Moon, D.H. Kim, Spatial Charge Separation On Strongly Coupled 2D-Hybrid of Rgo/$La_2Ti_2O_7$/Nife-Ldh Heterostructures for Highly Efficient Noble Metal Free Photocatalytic Hydrogen Generation, Applied Catalysis B: Environmental 239 (2018) 178-186.

[50] Y. Oaki, H. Imai, Chelation-Mediated Aqueous Synthesis of Metal Oxyhydroxide and Oxide

Nanostructures: Combination of Ligand-Controlled Oxidation and Ligandcooperative Morphogenesis, Chem.-Eur. J. 13 (2007) 8564-8571.

[51] L. Yu, Y. Zhang, J. He, H. Zhu, X. Zhou, M. Li, Q. Yang, F. Xu, Enhanced Photoelectrochemical Properties of A -Fe_2O_3 Nanoarrays for Water Splitting, J. Alloy. Compd. 753 (2018) 601-606.

[52] H. Cao, G. Wang, L. Zhang, Y. Liang, S. Zhang, X. Zhang, Shape and Magnetic Properties of Single‐Crystalline Hematite (A - Fe_2O_3) Nanocrystals, Chemphyschem 7 (2006) 1897-1901.

[53] K.K. Lee, P.Y. Loh, C.H. Sow, W.S. Chin, Coooh Nanosheet Electrodes: Simple Fabrication for Sensitive Electrochemical Sensing of Hydrogen Peroxide and Hydrazine, Biosens. Bioelectron. 39 (2013) 255-260.

[54] J. Liqiang, Q. Yichun, W. Baiqi, L. Shudan, J. Baojiang, Y. Libin, F. Wei, F. Honggang, S. Jiazhong, Review of Photoluminescence Performance of Nano-Sized Semiconductor Materials and its Relationships with Photocatalytic Activity, Sol. Energ. Mat. Sol. C. 90 (2006) 1773-1787.

[55] G.K. Pradhan, D.K. Padhi, K.M. Parida, Fabrication of A -Fe_2O_3 Nanorod/Rgo Composite: A Novel Hybrid Photocatalyst for Phenol Degradation, ACS Appl. Mater. Interfaces 5 (2013) 9101-9110.

[56] Z. Hua, X. Zhang, X. Bai, L. Lv, Z. Ye, X. Huang, Nitrogen-Doped Perovskite-Type $La_2Ti_2O_7$ Decorated On Graphene Composites Exhibiting Efficient Photocatalytic Activity Toward Bisphenol a in Water, Journal of Colloid and Interface Science 450 (2015) 45-53.

[57] L. Wang, B. Zhang, Q. Rui, Plasma-Induced Vacancy Defects in Oxygen Evolution Cocatalysts On Ta_3N_5 Photoanodes Promoting Solar Water Splitting, Acs Catal. 8 (2018) 10564-10572.

[58] C. Meng, M. Lin, X. Sun, X. Chen, X. Chen, X. Du, Y. Zhou, Laser Synthesis of Oxygen Vacancy-Modified Coooh for Highly Efficient Oxygen Evolution, Chem. Commun. 55 (2019) 2904-2907.

[59] D. Yang, A. Velamakanni, G. Bozoklu, S. Park, M. Stoller, R.D. Piner, S. Stankovich, I. Junga, D.A. Field, C.A.J. Ventrice, Chemical Analysis of Graphene Oxide Films After Heat and Chemical Treatments by X-Ray Photoelectron and Micro-Raman Spectroscopy, Carbon 47 (2009) 147-152.

[60] J.H. Kim, J.W. Jang, H.J. Kang, G. Magesh, J.Y. Kim, J.H. Kim, J. Lee, J.S. Lee, Palladium Oxide as a Novel Oxygen Evolution Catalyst On $Bivo_4$ Photoanode for Photoelectrochemical Water Splitting, J. Catal. 317 (2014) 126-134.

[61] X. Long, L. Gao, F. Li, Y. Hu, S. Wei, C. Wang, T. Wang, J. Jin, J. Ma, Bamboo Shoots Shaped $Fevo_4$ Passivated Zno Nanorods Photoanode for Improved Charge Separation/Transfer Process Towards Efficient Solar Water Splitting, Appl. Catal. B-Environ. 257 (2019)

[62] B. Klahr, S. Gimenez, F. Fabregat-Santiago, T. Hamann, J. Bisquert, Water Oxidation at Hematite Photoelectrodes: The Role of Surface States, J. Am. Chem. Soc. 134 (2012) 4294-4302.

[63] Z. Luo, C. Li, S. Liu, T. Wang, J. Gong, Gradient Doping of Phosphorus in Fe_2O_3 Nanoarray Photoanodes for Enhanced Charge Separation, Chem. Sci. 8 (2017) 91-100.

[64] L. Wang, F. Dionigi, T.N. Nhat, R. Kirchgeorg, M. Gliech, S. Grigorescu, P. Strasser, P. Schmuki, Tantalum Nitride Nanorod Arrays: Introducing Ni-Fe Layered Double Hydroxides as a Cocatalyst Strongly Stabilizing Photoanodes in Water Splitting, Chem. Mater. 27 (2015) 2360-2366.

[65] S. Shen, J. Zhou, C. Dong, Y. Hu, E.N. Tseng, P. Guo, L. Guo, S.S. Mao, Surface Engineered Doping of Hematite Nanorod Arrays for Improved Photoelectrochemical Water Splitting, Sci. Rep.-Uk 4 (2014)

[66] T. Soltani, A. Tayyebi, B. Lee, Efficient Promotion of Charge Separation with Reduced Graphene Oxide (Rgo) in $Bivo_4$/Rgo Photoanode for Greatly Enhanced Photoelectrochemical Water Splitting, Sol. Energ. Mat. Sol. C. 185 (2018) 325-332.

[67] G. Liu, J. Eichhorn, C. Jiang, M.C. Scott, L.H. Hess, J.M. Gregoire, J.A. Haber, I.D. Sharp, F.M. Toma, Interface Engineering for Light-Driven Water Oxidation: Unravelling the Passivating and Catalytic Mechanism in $Bivo_4$ Overlayers, SUSTAINABLE ENERGY & FUELS 3 (2019) 127-135.

[68] M. Zhang, R.P. Antony, S.Y. Chiam, F.F. Abdi, L.H. Wong, Understanding the Roles of Nio_x in Enhancing the Photoelectrochemical Performance of $Bivo_4$ Photoanodes for Solar Water Splitting, Chemsuschem 12 (2019) 2022-2028.

[69] I. Rodríguez-Gutierrez, E. Djatoubai, M. Rodríguez-Perez, J. Su, G. Rodríguez-Gattorno, L. Vayssieres, G. Oskam, Photoelectrochemical Water Oxidation at Fto|Wo_3@$Cuwo_4$ and Fto|Wo_3@$Cuwo_4$|$Bivo_4$ Heterojunction Systems: An Imps Analysis, Electrochim. Acta 308 (2019) 317-327.

[70] D. Klotz, D.A. Grave, A. Rothschild, Accurate Determination of the Charge Transfer Efficiency of Photoanodes for Solar Water Splitting, Phys. Chem. Chem. Phys. 19 (2017) 20383-20392.

[71] J. Zhang, R. Garcia-Rodriguez, P. Cameron, S. Eslava, Role of Cobalt-Iron (Oxy)Hydroxide ($Cofeo_x$) as Oxygen Evolution Catalyst On Hematite Photoanodes, Energ. Environ. Sci. 11

(2018) 2972-2984.

[72] Y. Makimizu, J. Yoo, M. Poornajar, N.T. Nguyen, H. Ahn, I. Hwang, S. Kment, P. Schmuki, Effects of Low Oxygen Annealing On the Photoelectrochemical Water Splitting Properties of A -Fe_2O_3, J. Mater. Chem. A 8 (2020) 1315-1325.

[73] S. Bai, X. Yang, C. Liu, X. Xiang, R. Luo, J. He, A. Chen, An Integrating Photoanode of Wo_3/Fe_2O_3 Heterojunction Decorated with Nife-Ldh to Improve Pec Water Splitting Efficiency, Acs Sustain. Chem. Eng. 6 (2018) 12906-12913.

[74] Y. Zhang, Y. Li, D. Ni, Z. Chen, X. Wang, Y. Bu, J. Ao, Improvement of $Bivo_4$ Photoanode Performance During Water Photo-Oxidation Using Rh-Doped $Srtio_3$ Perovskite as a Co-Catalyst, Adv. Funct. Mater. 29 (2019)

[75] Y. Ma, A. Kafizas, S.R. Pendlebury, F. Le Formal, J.R. Durrant, Photoinduced Absorption Spectroscopy of Copi On $Bivo_4$: The Function of Copi During Water Oxidation, Adv. Funct. Mater. 26 (2016) 4951-4960.

校对报告

当前使用的样式是 [journal of energy chemistry]

当前文档包含的题录共94条

有0条题录存在必填字段内容缺失的问题

所有题录的数据正常